Determination of Ti coordination from pre-edge peaks in Ti *K*-edge XANES

N. Jiang, D. Su, and J. C. H. Spence
Department of Physics, Arizona State University, Tempe, Arizona 85287-1504, USA
(Received 1 October 2007; published 26 December 2007)

The pre-edge peaks of Ti *K*-edge XANES have been widely used in determining Ti coordination in amorphous materials and in crystals despite the fact that coordination is not the only factor that the pre-edge peaks depend on. This work thoroughly examines the dependence of the shape of Ti *K* pre-edge peaks on various geometrical parameters (coordination, symmetry, Ti-O bond length and bond angle) using distorted rutile TiO_2 as models. We conclude that the greatest impact on the pre-edge peaks arises from a reduction in Ti-O bond length, although other parameters such as symmetry and coordination all have some effect.

DOI: 10.1103/PhysRevB.76.214117 PACS number(s): 61.10.Ht

I. INTRODUCTION

The local coordination of Ti^{4+} ions in silicate glasses and melts and in silica-supported titanium oxides has attracted much attention because of their unusual physical properties and applications for catalysis.[1,2] However, there are limited options available experimentally to quantify the coordination of Ti in amorphous materials. Along with other techniques, the x-ray absorption near-edge structure (XANES) of the Ti *K* edge has been widely used in probing the coordination of Ti in various crystalline and amorphous materials.[3–28] In tetrahedral coordination without inversion symmetry, Ti *K* edge XANES exhibits a strong pre-edge peak, while in octahedral coordination with inversion symmetry, Ti *K* edge only has a very weak or even no pre-edge absorption features. The earlier interpretations of these phenomena were based on molecular-orbital (MO) theory, which is a symmetry-based model for a cluster consisting of a Ti atom surrounded by its oxygen nearest neighbors.[29] According to the MO theory, the pre-edge peaks were due to a weak quadrupole $1s \rightarrow 3d$ transition. In the tetrahedron, the ligand field breaks the spherical symmetry of the atomic potential. This distortion changes the transition-matrix integral and, in effect, relaxes the dipole selection rules. Therefore, there is an increase in the strength of the $1s \rightarrow 3d$ quadrupole transition in tetrahedral versus octahedral compounds. This interpretation is still used in literature,[16,26] even though more sophisticated interpretations have been developed based on solid-state band theory, which indicates that the main features in the pre-edge region are not due to the dipole-forbidden $1s \rightarrow 3d$ transitions but due to Ti *p-d* mixing.[30–33] There is a fundamental difference between these two interpretations, although both rely on symmetry consideration. In experimental XANES, the dipole-forbidden features are angle dependent,[34] but the dipole-allowed features are not.

The confusion in interpretation does not interfere with the usefulness of the pre-edge features of Ti *K* XANES. In fact, the height and energy of the pre-edge peaks can be considered as fingerprints for qualitatively identifying Ti coordination in materials, for which it is not feasible to apply diffraction techniques, such as amorphous and nanoparticle samples. Farges *et al.* have even constructed a diagram of normalized peak height versus absolute position and defined three regions corresponding to tetrahedral (fourfold), square-pyramid (fivefold), and octahedral (sixfold) coordinated Ti.[32] These authors surveyed a large number of minerals with known structures and grouped the minerals with different Ti coordinations into three well-separated regions in the diagram. Although opinions differ toward the value of this diagram[21] and although the peak height also depends on the resolution of the apparatus,[20] the diagram has been widely used in qualitative or even quantitative assignment of Ti coordination in various materials.[12] In most silicate glasses or other Ti-containing amorphous materials, however, the normalized intensity and position of the Ti *K* pre-edge peak do not fall into any of those three defined regions. Therefore, the observed pre-edge peaks in these amorphous samples were often decomposed into reference spectra from selected crystals. Recently, there has been a tendency to use that diagram to quantify the fractions of Ti coordination in amorphous materials.[12] One approach is by fitting as the weighted average of two reference spectra.[5,14,19] However, this is valid only when there are two distinct Ti environments in the material.[28] A similar approach has been to deconvolute the pre-edge peaks by simple functions, such as Lorentz or Gaussian-Lorentz functions. The deconvoluted functions were assigned to different types of Ti coordination according to their positions; thus, the ratio of the population of different coordinations was obtained from the integrations of peaks.[12,20,25] All these simplified quantification attempts are called into question when we consider that the peak positions and peak intensity vary among compounds even with the same coordination. There is thus an underlying assumption in the use of the Ti pre-edge peak to determine coordination: that the Ti pre-edge appearance is only (or at least mainly) determined by the Ti coordination. Is this assumption always correct?

In this work, we have carried out a theoretical analysis of the dependence of the Ti *K* XANES pre-edge shape on various geometrical parameters, including coordination, symmetry and Ti-O bond length and bond angle. We begin with density functional theory (DFT) calculations based on the local density approximation for several typical Ti compounds, which provide an interpretation of Ti *K*-edge XANES in the pre-edge region. Symmetry considerations play an important role in Ti *p-d* mixing, and thus determine the key shape of the pre-edge feature. This is followed by a detailed discussion of the dependence of the pre-edge peak intensity upon the distortion of the Ti octahedron, where the

Ti-O bond lengths and bond angles and inversion symmetry were taken into account. We conclude by examining the notion that bond lengths in Ti polyhedra are more important than coordination in determining the pre-edge peak intensity.

II. THEORETICAL METHODS AND STRUCTURAL MODIFICATION

We used two complementary theoretical approaches in this work. Firstly, the pre-edge features of Ti *K* XANES were interpreted on the basis of the densities of states (DOSs) of Ti, which were calculated using the full potential linearized augmented plane wave (LAPW) plus local orbital method, obtained from the WIEN2K program.[35] The calculations were carried out in Ti compounds with different Ti coordinations, rutile TiO_2 (sixfold), $BaTiO_3$ (sixfold), $Ba_2TiSi_2O_3$ (fivefold), and Ba_2TiO_4 (fourfold). Secondly, simulations of Ti *K* XANES were carried out using the real-space multiple-scattering (MS) method using the FEFF8 program.[36] The main advantage of the full potential LAPW method is that it can calculate the DOS fairly accurately in regions near the Fermi level, which is considered to be the origin of the pre-edge peaks in the Ti *K* XANES. On the other hand, the real-space MS method has the freedom to manipulate atom positions in clusters, which is critical when investigating the dependence of the pre-edge peak intensity on the distortion of the Ti octahedron.

In the LAPW method, the basis set consists of muffin-tin (MT) orbitals; inside the nonoverlapping MT spheres, the basis functions are linear combinations of radial functions and their energy derivatives, while outside the spheres are plane waves. The basis functions and their first derivatives are continuous at the MT spheres. The Coulomb potential is expanded in the form $\Sigma_{lm}V_{lm}(r)Y_{lm}(\hat{\mathbf{r}})$ within the MT and $\Sigma_K V_K e^{i\mathbf{K}\cdot\mathbf{r}}$ in the interstitial region. For the exchange-correlation potential, the generalized gradient approximation was employed.[37] In the calculations, we used the experimental lattice parameters and atom positions. Relaxation of structure was not performed. The MT sphere radii (R) were 1.6 Å for the Ti and 1.5 Å for the O. Other parameters were $K_{\max}R_{\mathrm{MT}}=7.0$, where $K_{\max}$ is the plane-wave cutoff and R_{MT} is the smallest MT radius used in the calculation. 200–600 k points were used in the irreducible Brillouin zone, depending on different compounds.

In the real-space MS calculations, the Green's function was constructed using wave functions obtained by solving the Dirac equation self-consistently in the relativistic spinor representation using MT potentials. The Hedin-Lundqvist energy-dependent self-energy correction was added to the self-consistent Coulomb potential in the simulations of XANES. The radius of the cluster for full MS during the self-consistency loop is 4 Å, which contains about 20–25 atoms, whereas it is about 7–8 Å if it contains 180–200 atoms for the full MS XANES calculations. The maximum values of the angular momentum bases for both the self-consistent field and full multiple-scattering calculations are $l=1$ for O and 2 for Ti, respectively. The maximum value of the overlap for the muffin tins was 10%.

As mentioned above, quantifying the fraction of each Ti coordination in materials with possible mixed Ti coordinations relies on the validity of the assumption that the Ti local structure in amorphous material must be exactly the same as in crystals, or at least the small deviation from the rigid polyhedra found in crystals does not induce measurable changes in the pre-edge features. Obviously, the first assumption is invalid. Previous studies indicate that the bond lengths and angles in amorphous materials vary around average values, which may be close to the values in crystals.[38] Therefore, theoretical verification of the second assumption is necessary.

TABLE I. List of the local structures around Ti in various Ti-containing compounds (in Å).

Compound	Coordination	Longest Ti–O	Shortest Ti–O	Symmetry
c-$BaTiO_3$	Octahedral	2.00	2.00	O_h
t-$BaTiO_3$	Tetragonal	2.14	1.87	C_{4v}
Rutile TiO_2	Distorted octahedral	1.98	1.93	D_{2h}
$KTiOPO_4$	Distorted octahedral	2.15	1.73	
$Ba_2TiSi_2O_8$	Square pyramidal	1.97	1.70	
Ba_2TiO_4	Tetrahedral	1.82	1.63	
$Na_2TiOSi_4O_{10}$	Distorted octahedral	2.07	1.90	
$Na_2Ti_2Si_2O_9$	Distorted octahedral	2.18	1.82	
Na_2TiSiO_5	Square pyramidal	1.99	1.70	

The simulation of a real or probable amorphous structure is very challenging and complicated (or perhaps impossible?). A simple approach is to slightly modify the corresponding crystal structure by stretching or shortening bond lengths and tilting and twisting bond angles. Conceptually, such a distorted structure is not a glass, since the glass must be topologically different from the crystal. From a spectroscopic point of view, however, the distorted crystal structure is a fairly good model for simulating the effects of bond lengths and angles on absorption. This is because absorption is a localized phenomenon. Therefore, we can make the further simplification that we only distort the nearest neighbors of Ti. We therefore first construct two clusters around absorbing Ti atoms from a crystal structure. The bigger cluster includes about 200 atoms within a diameter of 0.7-1.0 nm, and the smaller cluster consists only of the absorbing Ti and the nearest neighboring O atoms. Then, we distort the small cluster by tilting, shifting, or removing O atoms relative to the absorbing Ti. The distorted small cluster is then embedded in the large cluster, replacing the absorbing Ti and its nearest neighbors. In this simple approach, the distortion is limited by the available space confined by the second-order nearest neighboring atoms of absorbing Ti. Certainly, the modified cluster is not at the lowest energy state, but neither is the glass.

Several crystal structures, including rutile TiO_2 and fresonite-type $Ba_2TiSi_2O_8$, were used in this work (Table I). In the rutile TiO_2, Ti is octahedrally coordinated to six oxygen atoms, two apical ($Ti\text{-}O_{ap}=1.98$ Å) and four equator oxygen ($Ti\text{-}O_{eq}=1.93$ Å). In the fresonite-type $Ba_2TiSi_2O_8$, Ti is located inside the square-pyramid polyhedron.

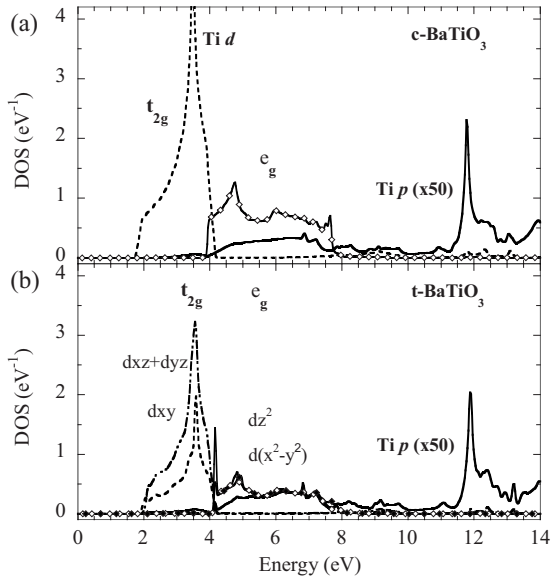

FIG. 1. Comparison of projected DOS of (a) cubic and (b) tetragonal $BaTiO_3$.

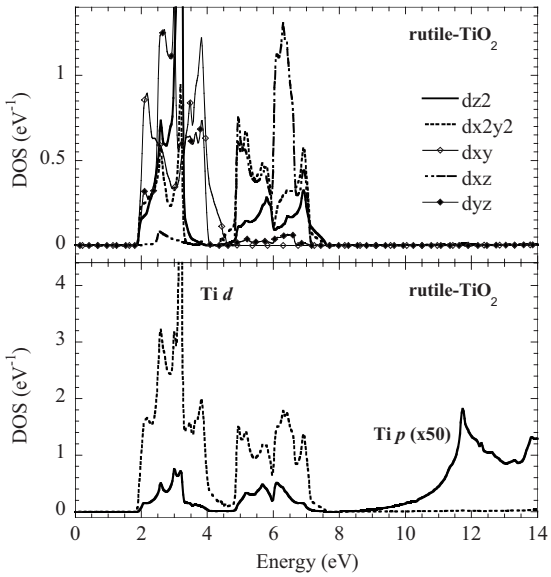

FIG. 2. Projected DOS of rutile TiO_2.

III. RESULTS AND DISCUSSION

A. Interpretation of the pre-edge features of Ti *K* x-ray absorption near-edge structure

The perfect Ti octahedral polyhedron has O_h symmetry. A representative compound of this case is cubic barium titanate (c-$BaTiO_3$). According to crystal-field theory, the O_h symmetry results in five d-type orbitals of Ti splitting into two groups.[39] The orbital d_{z^2} and $d_{x^2-y^2}$ point toward six equivalent oxygen atoms, while d_{xy}, d_{xz}, and d_{yz} point toward the midpoints of oxygen atoms. Therefore, the former two orbitals are degenerate and their unoccupied (antibonding) states have higher energy (denoted by e_g), while the latter degenerate three and their unoccupied states have lower energy (denoted by t_{2g}). This MO picture is consistent with more sophisticated band structure calculations. As shown in Fig. 1(a), the d band of c-$BaTiO_3$ splits into two subbands, corresponding to t_{2g} and e_g, respectively. For the Ti K XANES, the empty p band is located about 10-15 eV above the d band. The peaks below the p band consist of the pre-edge features of the Ti K XANES. In the literature, the commonly used pre-edge peaks for quantifying Ti coordination are those which overlap the d band. Therefore, we focus our discussion on the p states which overlap the d band. According to Fig. 1(a), the pre-edge feature of Ti XANES in c-$BaTiO_3$ is single peak with e_g characteristics, but its intensity is very weak.

Breaking the symmetry of O_h removes the degeneracy. In tetragonal barium titanate (t-$BaTiO_3$), Ti atoms shift slightly along the [001] direction, and thus the O_h symmetry reduces to C_{4v}. Under C_{4v} symmetry, d_{z^2} and $d_{x^2-y^2}$ become nondegenerate, and although d_{xz} and d_{yz} are still degenerate, they are different from d_{xy}. Since the displacement of Ti is very small, ~0.13 Å, as shown in Fig. 1(b), the differences between the nondegenerate states are very small. Correspondingly, the p states are similar between c- and t-$BaTiO_3$. In fact, the small differences in the p states may not be resolved by the Ti K XANES due to the intrinsic broadening by the Ti $1s$ core-hole lifetime and, thus, the pre-edge features of c- and t-$BaTiO_3$ should appear to be identical. Interestingly, the experimental pre-edge features of Ti K XANES in t-$BaTiO_3$ does not have the two-peak character as of rutile TiO_2 but a single weak peak.[40] Our calculations are consistent with this single-peak character. In perfect octahedral coordination or in C_{4v} symmetry, the O p state also perfectly degenerates into O $p(t_{2g})$ and O $p(e_g)$ without mixing with each other. The hybridization between Ti p and Ti t_{2g} neighboring states is suppressed because t_{2g} orbitals point toward the midpoints of oxygen atoms.

In rutile TiO_2, Ti is located at the center of a distorted oxygen octahedron, which is a special position with D_{2h} symmetry. The distortion includes two apical oxygen atoms (slightly extended), while four equatorial oxygen atoms are deformed from a square to a rectangle. Such a symmetry reduction from O_h to D_{2h} of an octahedron further breaks the degeneracy of the d orbitals; none of the five d orbitals is further degenerate, as shown in the top panel of Fig. 2. Correspondingly, the p-d mixing produces two weak peaks in the pre-edge region (bottom panel of Fig. 2). This is significantly different from the c- and t-$BaTiO_3$, although Ti atoms are in octahedral sites in all these cases. The reduction of point group symmetry in the distorted octahedron is responsible for this phenomenon. The lower symmetry allows some off-diagonal matrix elements (i.e., overlapping elements between different states) to become nonzero, which were zero in the higher symmetry.

Interestingly, rutile TiO_2 is often selected as a reference in the literature for octahedral Ti coordination, but not $BaTiO_3$. For example, the peak position and the integrated intensity of one of the two pre-edge peaks in rutile TiO_2 are often used as standard values to calculate the fraction of octahedrally coordinated Ti in amorphous and other materials of unknown structure. Although no reasons are given, one might expect

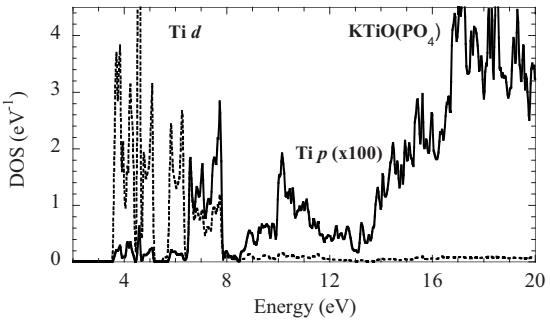

FIG. 3. Projected DOS of $KTiO(PO_4)$.

that O_h Ti octahedron in amorphous materials might be extremely rare. However, there are other symmetries lower than D_{2h} in the Ti octahedron. For example, in $KTiO(PO_4)$, the Ti octahedron is strongly asymmetric. It is remarkable that relative to rutile TiO_2, one of the two apical oxygen atoms become very close to Ti ($Ti\text{-}O_{ap} \sim 1.73$ Å), while the other moves apart ($Ti\text{-}O_{ap} \sim 2.15$ Å). This is due to the shift of Ti (0.403 Å) from the inversion center toward one of the apical oxygen atoms.[41] In addition, the angle of $O_{ap}\text{-}Ti\text{-}O_{ap}$ bonds is about 172°, rather than 180° as in rutile, producing a more distorted Ti octahedron. The calculations show that the p-DOS has strong mixing with e_g type of d-DOS, while the mixing with t_{2g} type is quite weak (Fig. 3). As a result, we can expect a single-peak pre-edge feature in the Ti K XANES. This is consistent with the experimental XANES in $KTiO(PO_4)$, which shows a quite strong single peak in the pre-edge region, and the intensity of this pre-edge peak increases with increasing distortion.[42] These results are significantly different from those observed in rutile TiO_2. Considering the distorted nature of amorphous material, one should therefore probably choose $KTiO(PO_4)$ to model the Ti octahedron in glasses rather than the more symmetric rutile TiO_2. However, the latter was overwhelmingly used as a reference in literature, without theoretical justification.

Experimentally, it is found that the pre-edge peaks of the Ti K-edge XANES are much stronger in Ti square-pyramidal and tetrahedral coordinations than in the octahedral. In the literature, this phenomenon was generally explained as due to lack of inversion centers in both square-pyramidal and tetrahedral coordinations. However, we cannot ignore the fact that "out-of-center" distortions[43] also exist in Ti octahedral coordination, some of which are quite large, such as in the above mentioned $KTiO(PO_4)$.

Figures 4 and 5 show the calculated DOS projected on Ti in examples of both square-pyramidal ($Ba_2TiSi_2O_8$) and tetrahedral (Ba_2TiO_4) coordinations, respectively. In $Ba_2TiSi_2O_8$, the basal plane of the TiO_5 square pyramid is undistorted.[44] Therefore, the d_{xz} and d_{yz} orbitals are degenerate. As shown in Fig. 4, the p state is orientation dependent. It is dominated by p_z character. Due to the symmetry, the mixing of p_x and p_y with d orbitals is quite weak. As a result, we can expect a narrow, single pre-edge peak of Ti K XANES in the square-pyramid Ti coordination. According to Fig. 4, p_z in the pre-edge region depends on d_{z^2}, while d_{z^2} depends strongly on the ratio between the axial and equatorial Ti-O bond lengths within the TiO_5 polyhedron.[45] Therefore, a distortion of the square-pyramid TiO_5 polyhedron can also affect the intensity of the pre-edge peak of the Ti K XANES.

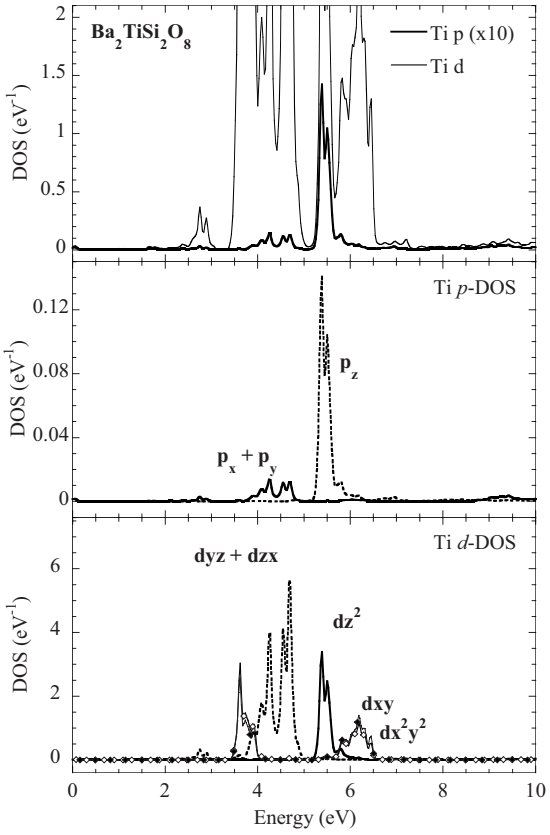

FIG. 4. Projected DOS of $Ba_2TiSi_2O_8$.

In Ba_2TiO_4, Ti is in tetrahedral coordination. It is seen that d orbitals are not degenerate. The p-d mixing is quite strong, and the p states in the pre-edge region are quite dispersive (Fig. 5). Therefore, the pre-edge peak in the Ti K XANES can be strong and broad. Relative to the cases in TiO_5, the peak position might be lower.

B. Dependence of pre-edge peak on distortion

In the previous section, we discussed the origins of the pre-edge peaks of Ti K XANES in various Ti coordinations. It is found that besides coordination, the appearance of the pre-edge features is also highly dependent on the symmetry of the Ti polyhedron. In this section, we discuss the relationship between distortion of Ti polyhedron and the pre-edge features. This becomes very important if the Ti K XANES is applied to amorphous materials. The nature of disorder in amorphous matter certainly guarantees the existence of various distorted Ti polyhedra, in which the Ti-O bond lengths and O-Ti-O bond angles differ from their values in any crystal. Experimentally, it has been known for years that the distortion of Ti octahedra in minerals has a strong effect on the appearance of the pre-edge intensity of Ti K XANES.[4] A brief theoretical investigation of the dependence of pre-edge peak intensity on distortion has been given by Ref. 46. Un-

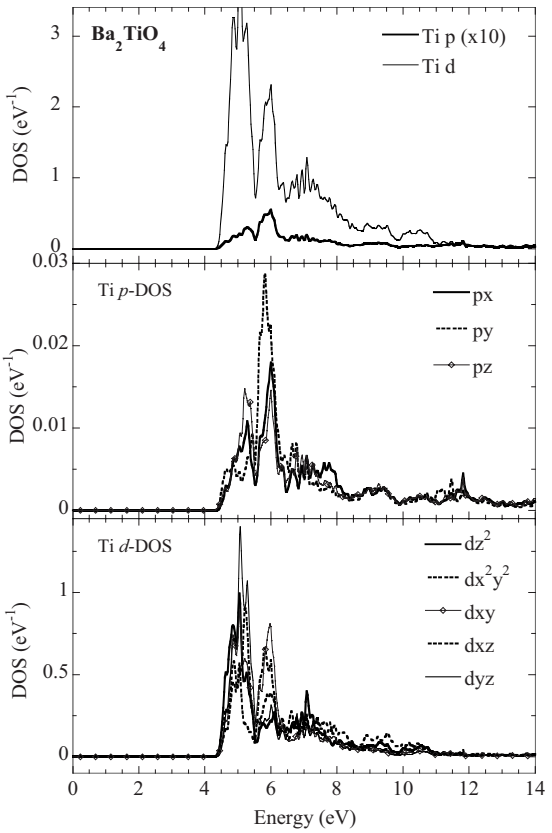

FIG. 5. Projected DOS of Ba_2TiO_4.

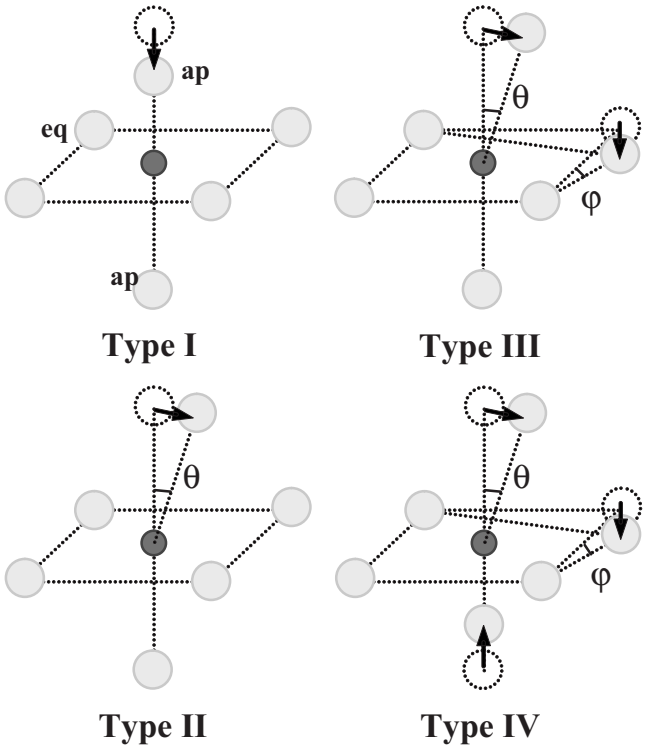

FIG. 6. Schematic drawings showing the distortion operations of Ti octahedron.

fortunately, the distortion effect has been ignored in recent attempts to quantify the coordination states of Ti in amorphous materials.

For simplicity, the embedded cluster model was used in this work. As mentioned above, the small slightly distorted Ti polyhedron was embedded into a large cluster, which was obtained from the experimental crystal structure. Figure 6 shows some examples of distorted Ti polyhedra constructed from the rutile Ti polyhedron. The distortion operations include shortening bond length between Ti and one apical oxygen atom (type I), tilting one apical O away from the apical axis (type II), type II operation plus tilting one equator O away from the equator plan (type III), and type III operation plus shortening the bond length between Ti with another apical oxygen (type IV). These distorted polyhedra then replace the central Ti polyhedron in a rutile TiO_2 cluster. This embedded model is certainly not an accurate model for the real disordered structure, unless the relaxation is allowed under certain constraints, but it can be quite effective for evaluating the possible effects of distortion on near-edge structure.

The pre-edge features in experimental Ti *K*-edge XANES of rutile TiO_2 consist of three peaks, which were called A1, A2, and A3 in literature. Our MS calculation only reproduces two peaks (A2 and A3) in the pre-edge region (Fig. 7). These two peaks are due to the dipole-allowed Ti $s \rightarrow p$ transitions with Ti $3d(t_{2g})$ and Ti $3d(e_g)$ characters, respectively.[47,48] The origin of peak A1 at the lowest energy has been controversial. The failure to reproduce A1 in most dipole-allowed calculations by different approaches[49,50] suggests that the quadrupole transition Ti $s \rightarrow d$ may be responsible for this peak. However, the cross section for the quadrupole transitions is negligibly small in our MS calculations, as is supported by some previous studies.[30] On the contrary, the angular dependent experimental XANES of the Ti *K* edge shows that the intensity of peak A1 is related to the orientation in a way which is characteristic of a quadrupole transition.[34,51–53] It was indicated that this weak peak A1 is probably due to the quadrupole excitonic transition.[54] In

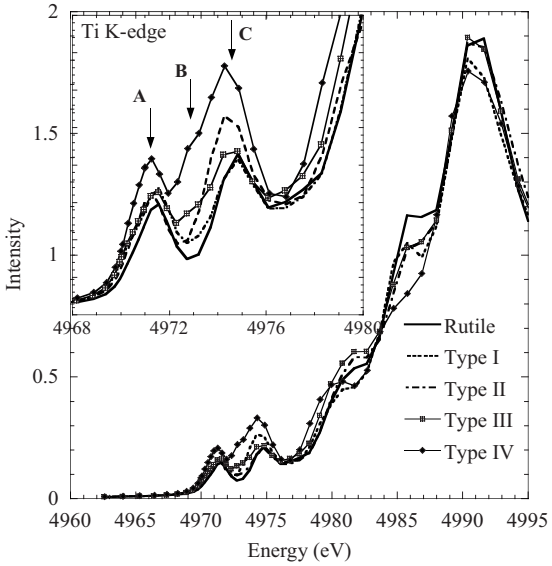

FIG. 7. Comparison of distortion effects on Ti *K* pre-edge peaks. Four types of distortion are given in Fig. 6.

short, the interpretation of all three pre-edge peaks of rutile TiO_2 is still a challenge to theoretical models. Fortunately, this weak peak A1 of rutile TiO_2 is rarely seen in other Ti compounds and is not involved in Ti coordination determinations in the literature. Therefore, we only focus our discussion on the dipole-allowed transitions in this work.

In Fig. 7, it is clearly seen that some distortions of the nearest neighbors around Ti alone can significantly induce changes in the Ti *K* XANES, not only in the pre-edge region but also in the main peaks. The octahedral distortion effect on the main peaks in rutile TiO_2 has been discussed previously.[55] Here, we will only focus on the changes in the pre-edge region.

Among these distortions, only types II and III involve tilting operations, while both types I and IV have a short Ti-O bond. It is seen that slightly tilting the oxygen away from the apical axis and off the equator has little effect on the pre-edge features, although an off-plane equator oxygen may induce a small intensity (indicated as B) between two rutile peaks (A and C). On the contrary, a short Ti-O bond length can strongly enhance the intensity of peak C. Combined with an off-plane equator oxygen, it also creates a strong shoulder between peaks A and C. These results indicate that the distortion induced merely by varying bond angles may not have a strong effect on the pre-edge appearance. This phenomenon can be explained as follows: the slight change in bond angle may reduce the symmetry, but it does not have much effect on the orbital overlap between Ti and O atoms. In other words, the Ti-O bonding character is not changed significantly by a slight change of bond angle. This is very different from a bond length change. A short Ti-O bond can significantly alter the orbital overlap and thus cause the bonding character to change from ionic to a covalent. Usually, a short Ti-O bond exists in the square-pyramid fivefold Ti polyhedron. It is interesting that a short Ti-O bond does exist in Ti octahedral coordination as well, such as in ferroelectric $MTiO(PO_4)$ isomorphous compounds, in which there is one short and one long Ti-O bonds along the apical axis.[56] Therefore, in terms of the pre-edge appearance of Ti *K* XANES, the distortion of Ti octahedra can be practically defined as the difference between the long and short Ti-O distances. This notion has also been used in some earlier experimental papers.[4]

According to this definition of distortion, Fig. 8 shows the dependence of the pre-edge appearance of Ti *K* XANES with distortion. The degree of distortion is listed in Table II. It is clearly seen that the intensity of peak C increases with increasing distortion. In addition, the peak position also shifts slightly toward lower energy with increasing distortion. In the case of type I-ap4 (Fig. 8), the pre-edge feature becomes dominated by a single peak with a shoulder on the low energy side, rather than the two-peak character. These results are consistent with the experimental results in the isomorphous $KTiOPO_4$, in which the pre-edge features are dominated by a single strong peak, and the peak intensity increases with increasing distortion.[42] It is also noted that the distortion of Ti polyhedra mainly induces a change in the second dipole transition peak (peak C), i.e., the e_g-type peak. This is probably because the change in the absorption is mainly induced by the short Ti-O distance (types I and IV in Fig. 6). We also note that this result, based on MS theory (FEFF), is also consistent with the DFT calculations (WIEN), in which the highly distorted Ti octahedron results in a strong e_g-type empty DOS (Fig. 3).

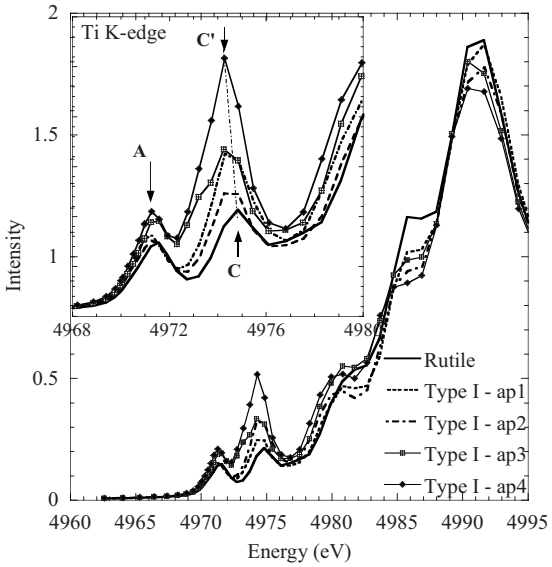

FIG. 8. Comparison of distortion degree on Ti *K* pre-edge peaks. The distortion degree is defined in Table II.

Besides bond length and angle, another important parameter is the location of the central Ti in the polyhedron. An off-center distortion is quite common in the Ti octahedra. For example, Ti shifts about 0.13 Å off the center along the *z*-axis in the *t*-$BaTiO_3$. To compare the impact on the pre-edge appearance of the off-center distortion with the shorter Ti-O bond length, we create two distorted Ti octahedra from rutile TiO_2. One model shifts four equatorial oxygen atoms 0.3 Å along one apical direction [Fig. 9(a)]. In this case, the Ti-O bond lengths do not change significantly from the normal rutile structure, but the Ti is not located at the center, and thus there is no inversion symmetry in this new octahedron. Another model shifts one apical oxygen atom toward the central Ti along with the four equatorial oxygens. In this case, one Ti-O bond becomes short and Ti is off center [Fig. 9(b)]. The computational results of these two models are compared in Fig. 10 with calculations for the normal rutile structure. Surprisingly, the off-center distortion alone has little effect on the pre-edge appearance. On the other hand, however, adding a short Ti-O bond to the distortion tends to create a single strong peak. This result is consistent with the

TABLE II. Definition of the degree of distortion of an octahedron (in Å). The distortion operation of type I is defined in Fig. 6. Both oxygen in short and long Ti–O refer to apical oxygen.

	Ti–O (short)	Ti–O (long)	Difference
Type I-ap1	1.8	2.0	0.2
Type I-ap2	1.7	2.0	0.3
Type I-ap3	1.8	2.2	0.4
Type I-ap4	1.7	2.2	0.5

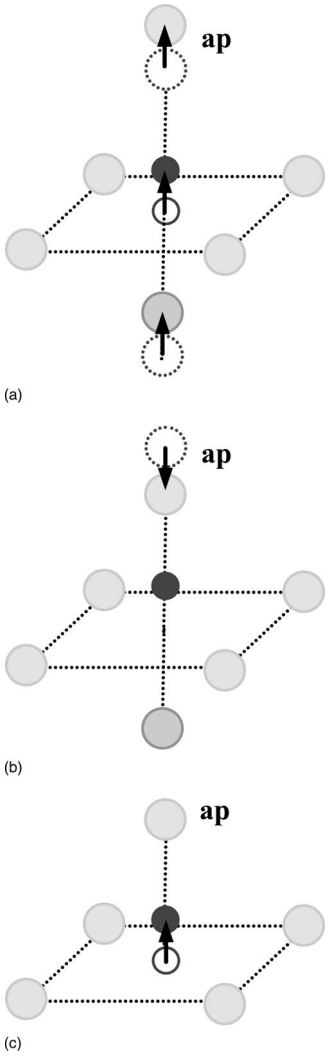

FIG. 9. (a) Construction of octahedron with off-center Ti. (b) Off-centered octahedron with a short Ti-O distance. (c) Construction of a square-pyramid polyhedron from an octahedron.

calculations and experiments in the t-$BaTiO_3$, in which the short Ti-O bond length is 1.8 Å.

In short, among the possible distortions of Ti octahedron, a short bond length has the most significant impact on the appearance of the pre-edge features of Ti K XANES, while the coordination and the symmetry are less important. In some of the octahedral Ti compounds, the distorted Ti octahedron includes at least one short Ti-O bond. In these cases, the experimental Ti K XANES always shows strong-single peak pre-edge features, and the peak intensity depends on the distortion, which can be measured by the difference between the longest and the shortest Ti-O bond length in the octahedron. According to this definition, the square-pyramid Ti polyhedron can be considered as the most distorted "octahedron," in which the shortest Ti-O distance is between 1.6 and 1.7 Å, while the longest one is "infinite." This hypothesis can be demonstrated by comparing the Ti K-edge XANES in three sodium titanium silicates, $Na_2TiOSi_4O_{10}$, $Na_2Ti_2Si_2O_9$, and Na_2TiSiO_5 (Fig. 11). In $Na_2TiOSi_4O_{10}$, the Ti octahedron is very similar to that in rutile, although one Ti-O_{ap} is

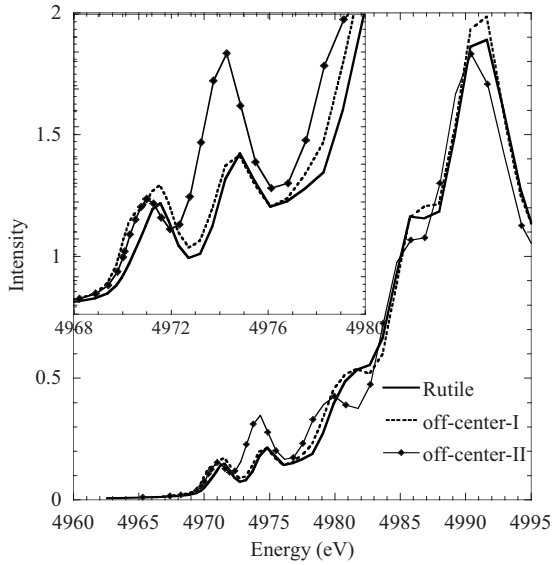

FIG. 10. Comparison of off-center effect with a reduction of Ti-O bond length.

shorter than another. The difference is about 0.17 Å. In $Na_2Ti_2Si_2O_9$, however, the Ti octahedron is very irregular and distorted. The difference between the longest and shortest Ti-O distances is more than 0.36 Å. As expected, the pre-edge appearance in the $Na_2TiOSi_4O_{10}$ is very similar to that in the rutile (Fig. 11), while it develops a single-peak character in $Na_2Ti_2Si_2O_9$. In Na_2TiSiO_5, the Ti polyhedron is a square pyramid, in which the shortest Ti-O is only 1.69 Å. In this case, the pre-edge feature is completely dominated by a very strong single peak (Fig. 11).

These calculations raise questions about whether the pre-edge appearance is more sensitive to the coordination or something else, such as the shortest bond length in the Ti polyhedron. No doubt, all the geometric parameters will

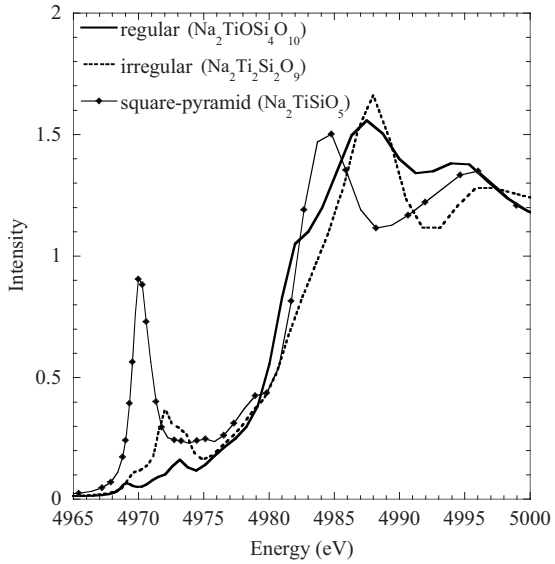

FIG. 11. Comparison of Ti K pre-edge features in different Ti polyhedrons in the sodium titanium silicates.

have some impact on the pre-edge features, but a short Ti-O bond length seems to have the most influence. Although there is a certain relation between the coordination and the bond lengths, one cannot just simply rule out a possible very short Ti-O bonding length in a much distorted Ti octahedron. A brief survey of the Ti *K* XANES shows that the pre-edge appearance in Ti-containing amorphous material is barely similar to that in the rutile. A single peak with various intensities was always observed.[12,13] In these cases, one cannot simply rule out any coordination or the combination of two or three coordinations.

Finally, we would like to comment on the validity of the distortion models used in this study. As mentioned above, the distorted Ti octahedra in the rutile structure are artificial and may not be in the lowest energy state. Therefore, we do not expect the calculations for these distorted models to match any experimental data quantitatively. However, the effects of distortion on the appearance of the pre-edge features of Ti *K* XANES can be qualitatively demonstrated by these models. Figure 12 is an example showing the validity of this effect. We constructed a square-pyramid polyhedron around Ti in the rutile Ti octahedron [Fig. 9(c)]. By doing this, we shifted the Ti away from the center about 0.3 Å toward one apical oxygen atom along the apical axis and deleted the other apical oxygen. In this artificial Ti square pyramid, one Ti-O_{ap} is about 1.68 Å, four Ti-O_{eq} are about 1.97 Å, and Ti is 0.3 Å above the bottom plane. These parameters are similar to the "real" Ti square-pyramid polyhedron in $Ba_2TiSi_2O_8$. The calculated Ti *K*-edge XANES in this modified structure is compared with the calculations of $Ba_2TiSi_2O_8$ and rutile TiO_2 in Fig. 12. Surprisingly, the spectrum of the artificial Ti square-pyramid polyhedron is very similar to that of $Ba_2TiSi_2O_8$, although the absolute energies of the two spectra are different. This is probably due to the different chemistries in these two structures. This result demonstrates that the general appearance of Ti *K* XANES is more sensitive to the geometry of the nearest neighbors of the Ti than the chemistry of the structure.

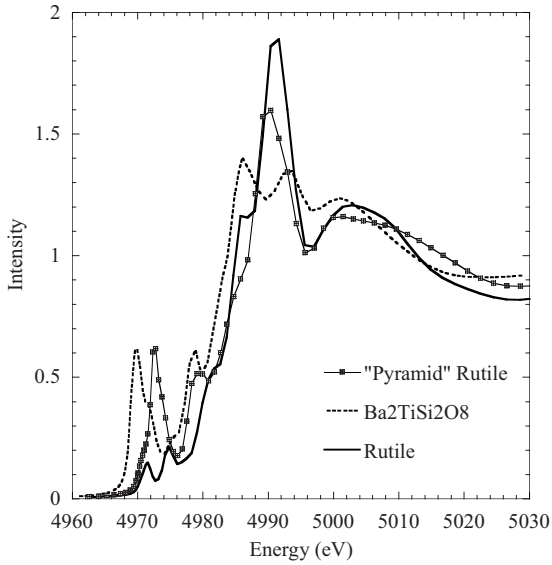

FIG. 12. Comparison of constructed Ti square-pyramid polyhedron with the real one in $Ba_2TiSi_2O_8$.

IV. CONCLUSION

An interpretation of Ti *K* XANES for various Ti coordinations has been given, based on DFT calculations using the full potential LAPW code WIEN2K. Both the main peak and the pre-edge peaks of the Ti *K* XANES are determined by the unoccupied Ti *p*-DOS. The pre-edge features are mainly induced by Ti *p*-*d* mixing, mediated by the nearest neighbor oxygen and, thus, the appearance of the pre-edge features depends on the geometry of the Ti polyhedron. The influence of atoms beyond the nearest neighbors was not examined in this study.

Furthermore, the impact of various geometric parameters on Ti *K* pre-edge features has been evaluated based on calculations using the real-space full multiple-scattering code FEFF8. It is found that the greatest impact on the pre-edge features arises from a reduction in Ti-O bond length, although other parameters, such as symmetry, coordination, and angles, all have some effect. Therefore, we should be cautious about using the Ti pre-edge peak(s) to determine Ti coordination.

ACKNOWLEDGMENT

This work was supported by NSF DMR 0603993.

[1] G. E. Brown, F. Farges, and G. Calas, Rev. Mineral. **32**, 317 (1995), and references therein.
[2] X. Gao and I. E. Wachs, Catal. Today **51**, 233 (1999).
[3] R. B. Greegor, F. W. Lytle, D. R. Sandstrom, J. Wong, and P. Schultz, J. Non-Cryst. Solids **55**, 27 (1983).
[4] G. A. Waychunas, Am. Mineral. **72**, 89 (1987).
[5] P. Behrens, J. Felsche, S. Vetter, G. Schulz-Ekloff, N. I. Jaeger, and W. Niemann, J. Chem. Soc., Chem. Commun. **1991**, 678.
[6] T. Blasco, M. A. Camblor, A. Corma, and J. Perez-Pariente, J. Am. Chem. Soc. **115**, 11806 (1993).
[7] S. Quartieri, G. Antonioli, G. Artioli, and P. P. Lottici, Eur. J. Mineral. **5**, 1101 (1993).
[8] D. B. Dingwell, E. Paris, F. Seifert, A. Mottana, and C. Romano, Phys. Chem. Miner. **21**, 501 (1994).
[9] C. W. Ponader, H. Boek, and J. E. Dickinson, Jr., J. Non-Cryst. Solids **201**, 81 (1996).
[10] F. Farges, G. E. Brown, and J. Rehr, Geochim. Cosmochim. Acta **60**, 3023 (1996).
[11] F. Farges, Am. Mineral. **82**, 36 (1997); **82**, 44 (1997).
[12] G. Mountjoy, D. M. Pickup, G. W. Wallidge, R. Anderson, J. M. Cole, R. J. Newport, and M. E. Smith, Chem. Mater. **11**, 1253 (1999).
[13] C. Romano, E. Paris, B. T. Poe, G. Giuli, D. B. Dingwell, and A. Mottana, Am. Mineral. **85**, 108 (2000).
[14] W. B. Kim, S. H. Choi, and J. S. Lee, J. Phys. Chem. B **104**, 8670 (2000).

[15] D. M. Pickup, G. Mountjoy, M. A. Holland, G. W. Wallidge, R. J. Newport, and M. E. Smith, J. Phys.: Condens. Matter **12**, 9751 (2000).
[16] J. Xu, A. P. Wilkinson, and S. Pattanaik, Chem. Mater. **12**, 3321 (2000); J. Xu, C. Lind, A. P. Wilkinson, and S. Pattanaik, *ibid.* **12**, 3347 (2000).
[17] A. Hagen, K. Schueler, and F. Roessner, Microporous Mesoporous Mater. **51**, 23 (2002).
[18] V. V. Kriventsov, D. I. Kochubey, M. V. Tsodikov, J. A. Navio, G. M. Restrepo, and M. Macias, Nucl. Instrum. Methods Phys. Res. A **470**, 347 (2001); V. V. Kriventsov, D. I. Kochubey, M. V. Tsodikov, and J. A. Navio, *ibid.* **470**, 331 (2001).
[19] T. Tanaka, K. Teramura, T. Yamamoto, S. Takenaka, S. Yoshida, and T. Funabiki, J. Photochem. Photobiol., A **148**, 277 (2002).
[20] H. Yoshitake, T. Sugihara, and T. Tatsumi, Phys. Chem. Chem. Phys. **5**, 767 (2003).
[21] M. Bandyopadhyay, A. Birkner, M. V. E. van den Berg, K. V. Klementiev, W. Schmidt, W. Grunert, and H. Gies, Chem. Mater. **17**, 3820 (2005).
[22] S. Matsuo, N. Sakaguchi, and H. Wakita, Anal. Sci. **21**, 805 (2005).
[23] S. D. George, P. Brant, and E. I. Solomon, J. Am. Chem. Soc. **127**, 667 (2005).
[24] G. Dutta, U. V. Waghmare, T. Baidya, M. S. Hegde, K. R. Priolkar, and P. R. Sarode, Chem. Mater. **18**, 3249 (2006).
[25] T. L. Hsiung, H. P. Wang, and H. C. Wang, Radiat. Phys. Chem. **75**, 2042 (2006).
[26] S. D. George, K. Huang, R. W. Waymouth, and E. I. Solomon, Inorg. Chem. **45**, 4468 (2006).
[27] J. Park, J. Yang, J. Yoon, S. Hwang, and J. Choy, J. Phys. Chem. B **110**, 1592 (2006).
[28] G. Mountjoy, D. M. Pickup, R. J. Newport, and M. E. Smith, J. Phys. Chem. B **105**, 6273 (2001).
[29] L. A. Grunes, Phys. Rev. B **27**, 2111 (1983).
[30] B. Poumellec, P. J. Durham, and G. Y. Duo, J. Phys.: Condens. Matter **3**, 8195 (1991).
[31] Z. Y. Wu, G. Ouvard, P. Gressier, and C. R. Natoli, Phys. Rev. B **55**, 10382 (1997).
[32] F. Farges, G. E. Brown, and J. J. Rehr, Phys. Rev. B **56**, 1809 (1997).
[33] G. Fronzoni, R. De Francesco, M. Stener, and M. Causa, J. Phys. Chem. B **110**, 9899 (2006).
[34] T. Uozumi, K. Okada, A. Kotani, O. Durmeyer, J. P. Kappler, E. Beaurepaire, and J. C. Parlebas, Europhys. Lett. **18**, 85 (1992).
[35] P. Blaha, K. Schwarz, G. K. H. Madsen, D. Kvasnicka, and J. Luitz, WIEN2K, an augmented plane wave+local orbitals program for calculating crystal properties, Karlheinz Schwarz, Technical Universität Wien, Austria, 2001.
[36] A. L. Ankudinov and J. J. Rehr, Phys. Rev. B **62** 2437 (2000).
[37] J. P. Perdew, K. Burke, and M. Ernzerhof, Phys. Rev. Lett. **77**, 3865 (1996).
[38] For a review, see P. H. Gaskell, in *Materials Science and Technology*, edited by R. W. Cahn (VCH, Weinheim, 1991).
[39] S. Sugano, Y. Tanabe, and H. Kamimura, *Multiplets of Transition-Metal Ions in Crystals* (Academic, New York, 1970).
[40] A. I. Frenkel, Y. Feldman, V. Lyahovitskaya, E. Wachtel, and I. Lubomirsky, Phys. Rev. B **71**, 024116 (2005).
[41] I. Tordjman, R. Masse, and J. C. Guitel, Z. Kristallogr. **139**, 103 (1974).
[42] B. Pillep, M. Froba, M. L. F. Phillips, J. Wong, G. D. Stucky, and P. Behrens, Solid State Commun. **103**, 203 (1997).
[43] M. Kunz and I. D. Brown, J. Solid State Chem. **115**, 395 (1995).
[44] T. Hoche, W. Neumann, S. Esmaeilzadeh, R. Uecker, M. Lentzen, and C. Russel, J. Solid State Chem. **166**, 15 (2002).
[45] T. Hoche, F. Heyroth, M. Grodzicki, and P. A. van Aken, Phys. Status Solidi A **202**, 2355 (2005).
[46] E. Paris, C. Romano, and Z. Wu, Physica B **208&209**, 351 (1995).
[47] R. Brydson, H. Sauer, W. Engel, J. M. Thomas, E. Zeitler, N. Kosugill, and H. Kurodall, J. Phys.: Condens. Matter **1**, 797 (1989).
[48] M. F. Ruiz-Lopez and A. Munoz-Paez, J. Phys.: Condens. Matter **3**, 8981 (1991).
[49] G. Fronzoni, R. De Francessco, M. Stener, and M. Causa, J. Phys. Chem. B **110**, 9899 (2006).
[50] J. Chaboy, N. Nakajima, and Y. Tezuka, J. Phys.: Condens. Matter **19**, 266206 (2007).
[51] B. Poumellec, R. Cortes, G. Tourillon, and J. Berthon, Phys. Status Solidi B **164**, 319 (1991).
[52] Y. Joly, D. Cabaret, H. Renevier, and C. R. Natoli, Phys. Rev. Lett. **82**, 2398 (1999).
[53] T. Uozumi, A. Kotani, and J. C. Parlebas, J. Electron Spectrosc. Relat. Phenom. 1 **37-140**, 623 (2004).
[54] E. L. Shirley, J. Electron Spectrosc. Relat. Phenom. **136**, 77 (2004).
[55] V. Jeane-Rose and B. Poumellec, J. Phys.: Condens. Matter **11**, 1123 (1999).
[56] G. D. Stucky, M. L. F. Phillips, and T. E. Gier, Chem. Mater. **1**, 492 (1989).